ACS Sustainable Chemistry & Engineering

pubs.acs.org/journal/ascecg

Research Article

From Solution to Microstructures in Minutes: Microdroplet-Derived Stand-Alone TiO_2 Surfaces for Simultaneous Water Harvesting and Treatment

Keerthana Unni, Jenifer Shantha Kumar, Anirban Som, Depanjan Sarkar,* and Thalappil Pradeep*

Cite This: https://doi.org/10.1021/acssuschemeng.4c02806

Read Online

ACCESS | Metrics & More | Article Recommendations | Supporting Information

ABSTRACT: We present a straightforward and eco-friendly method to transform a titanium tetraisopropoxide (TTIP) solution into superhydrophobic TiO_2 microstructures by ambient microdroplet deposition. At lower temperatures the micropillars of amorphous TiO_2 act as nucleation sites for condensing humidity to form droplets. However, the microstructures facilitate efficient water runoff despite TiO_2's hydrophilic character by a combination of surface hydrophobicity and gravity. Additionally, the photocatalytic TiO_2 surface resists biofilm formation and degrades the contaminants, offering long-term collection of safe water and its purification, which has been demonstrated with examples. We demonstrate that the microdroplet-based methodology developed for the conversion of solution into microdroplets can also be applied to other metal oxides, including CuO and ZnO, highlighting the universality of the process.

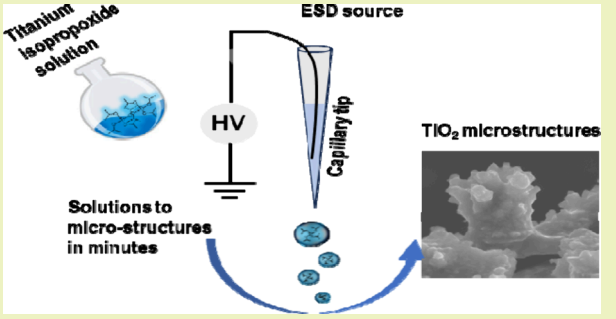

KEYWORDS: *Electrospray deposition, Ambient microdroplets, Microstructures, TiO_2, Atmospheric water harvesting, Photocatalysis,, Antibacterial property, Titanium tetraisopropoxide*

INTRODUCTION

Microdroplets have emerged as a powerful medium for rapid synthesis of molecules[1−8] and materials.[9−18] Such methods are sustainable means of synthesis as they require minimum reagents and minimal or no activating agents such as acids, catalysts, etc., are used.[5] Electrospray deposition (ESD) of microdroplets is a powerful way of creating nanostructures for diverse applications.[13,19] This paper explores the use of microdroplets to address one of humanity's most important problems, namely clean water, using microdroplet-derived nanostructures.

As the world's population grows and living standards improve, clean water is becoming a major challenge for sustainable development. Safe drinking water is a fundamental human right, yet millions lack its access, leading to devastating health consequences. Additionally, industries and agriculture are highly dependent on water resources, and shortages can lead to economic recession and food insecurity.[20] Equally alarming is the contamination of water sources, rendering even existing water supplies unsuitable for consumption.[21−29] Tackling the global water crisis requires a comprehensive strategy that includes efficient conservation, responsible management, development of innovative purification and desalination technologies and appropriate investment.[30−36] Establishing alternative water sources is a crucial aspect of making clean water accessible to all.[37] Atmospheric water capture (AWC) has emerged as a potential solution to provide clean water to regions with scant natural water resources.[38−48] This is primarily because, at any specific time, the Earth's atmosphere holds an astonishing 37.5 million billion gallons of water in the vapor form,[49] and an effective, cost-efficient device capable of capturing a portion of this could contribute to addressing the water crisis.

Microstructured surfaces have emerged as an important innovation in water harvesting.[19,50−53] These surfaces are meticulously designed with tiny, engineered structures that effectively capture and channel water droplets, making them particularly adept at harvesting water from the atmosphere. We had reported the creation of biomimicked hydrophilic−hydrophobic patterned microstructured surfaces with unprecedented water harvesting efficiency.[19] By exploiting principles of condensation and wettability, microstructured surfaces encourage water vapor to condense into droplets, which are then rapidly transported and collected for various purposes, from potable water supplies to irrigation. Over the past decade, there has been renewed interest in developing microstructured

Received: April 3, 2024
Revised: July 8, 2024
Accepted: July 8, 2024

surfaces for water harvesting.[54−56] However, many existing fabrication methods use complex instrumentation such as atom bombardment and electron beam lithography.[57−59] In addition to their complex fabrication procedures, these surfaces encounter challenges related to extended usage for various reasons, such as substrate material leaching, contamination by volatile organic compounds, dyes, and biofilm formation. Recent research has demonstrated that TiO_2, owing to its photocatalytic properties, can serve as a material for creating surfaces for AWC capable of both water harvesting and contamination removal simultaneously. However, these substrates typically utilize TiO_2-embedded polymers, which can suffer from leaching issues. Thus, there is a pressing need to develop TiO_2 surfaces with microstructures that do not rely on supporting chemicals for effective AWC and treatment.[60]

ESD offers an accessible and practical means of fabricating microstructured surfaces for efficient water harvesting. Another vital consideration in the development of effective water harvesting surfaces is the ability to ensure long-term reusability with acceptable efficiency.[60] Several factors come into play when assessing a surface's suitability for extended use, with surface stability under varying conditions being an aspect of paramount importance. One significant challenge lies in preserving the surface's stability when exposed to a range of environmental factors and potential contaminants from the atmosphere, which can diminish its capacity to provide clean water effectively. Additionally, the formation of biofilms on these surfaces can act as a hindrance to their extended use. Addressing these issues is pivotal for creating water harvesting surfaces with sustained efficiency and long-term reusability.

Here, we introduce an innovative, environment friendly, and straightforward approach for seamlessly transforming a titanium isopropoxide solution into extensive microstructures of titanium dioxide (TiO_2) under standard atmospheric conditions. These microstructures were deliberately designed in such a way that they collectively induce superhydrophobicity on the surface, allowing water to roll off effortlessly despite TiO_2's intrinsic hydrophilic nature.[61] When the surface was cooled, the hydrophilic micropillars made of TiO_2 served as nucleation sites for water droplets. Subsequently, the combined influence of the surface's hydrophobic nature and the force of gravity allowed for the easy roll-off of the water droplets. Furthermore, TiO_2 has photocatalytic properties,[62] rendering it self-cleaning and resistant to biofilm formation when exposed to sunlight. This quality ensures prolonged safe use of the surface while also enabling the degradation of contaminants such as organic dyes and drug molecules, offering a means to purify the collected water, if ambient contaminants are present. Consequently, this engineered surface demonstrates an exceptional ability to independently collect and purify water from the atmosphere simultaneously. This approach was expanded to include other metal oxides, demonstrating its universality in creating microstructures from corresponding solutions within min.

MATERIALS AND METHODS

Materials Used. TTIP, copper acetate monohydrate, zinc acetate dihydrate, rhodamine 6G, methylene blue, rhodamine B, and ibuprofen were purchased from Sigma-Aldrich, India. Indium tin oxide glass slides were bought from Toshniwal Brothers (SR) Pvt. Ltd., India. Stainless steel (SS) mesh was acquired from eBay and was used as the surface to grow the microstructures. Copper TEM grids were sourced from SPI Supplies. Micropipette puller (P-97) and glass capillaries for nanoelectrospray (nESI) were purchased from Sutter Instrument, USA. Milli-Q water was used for all the experiments. Nutrient agar (NA) and Luria−Bertani (LB) Broth for bacteria culture were purchased from HiMedia.

Instrumentation. Morphologies of microstructures formed using electrospray deposition were analyzed using a Thermo Scientific Verios G4 UC High-Resolution Field Emission Scanning Electron Microscope (HR-FESEM). Prior to imaging, samples were given a gold coating. Energy-dispersive spectroscopy (EDS) was used to analyze the microstructure composition. The static contact angle of the surfaces was measured using the GBX Digidrop contact angle meter. High-Resolution Transmission Electron Microscopy (HR-TEM) measurements were performed using a JEOL 3010 instrument. Thermo Scientific LTQ − XL mass spectrometer was used for analyzing the photocatalysis products. Keyence VHX-950F was used to capture the images of water harvesting experiments. Olympus IX83 inverted fluorescence microscope was used to evaluate the antibacterial activity of TiO_2 microstructures.

Electrospray Deposition. Homemade nanoelectrospray emitters were fabricated using glass capillaries with outer diameters (ODs) of 1.5 mm and inner diameters (IDs) of 0.86 mm. The micropipette puller settings were meticulously optimized to produce pulled tips with openings ranging from 30 to 40 μm. Each tip was thoroughly examined under an optical microscope, and any tips that deviated from the specified dimensions or with defects were discarded. The glass emitter tips were carefully filled with the desired precursor solutions using Eppendorf pipet tips. Subsequently, a platinum (Pt) wire (purchased from Sigma-Aldrich) with a diameter of 0.1 mm was employed to establish electrical connectivity. The nESI assembly was then connected to an external high-voltage source powered by a variable DC power supply (purchased from Sunmach Equipment) using a copper alligator clip. Upon applying a potential of 1−1.30 kV, a spray plume consisting of charged microdroplets was seen emanating from the tip of the emitter. This spray plume was directed toward a grounded electrode composed of a SS mesh of 74 μm mesh-size positioned on an ITO glass slide for neutralization and collection of the generated ions. The distance between the collector surface and the nESI emitter was 8−10 mm. All the parameters, like the distance and voltage, were optimized using trial and error method.

Fabrication of Microstructures Using Electrospray Deposition (ESD) of Microdroplets. First a homogeneous solution of the desired precursor in dry ethanol was prepared. It was then subjected to ESD, where the spray was deposited onto a dedicated SS mesh positioned on a grounded ITO plate. The duration of the ESD process varied from 60 to 120 min depending on the specific objectives of the experiment. Finally, the SS mesh underwent a low-temperature annealing step (100−120 °C) for an hour in a hot air oven, completing the transformation.

Water Harvesting Using Hydrophobic−Hydrophilic TiO_2 Microstructures. To investigate the water capture capabilities of the ESD-synthesized TiO_2 microstructure surfaces, a 1 cm × 1 cm SS mesh with the desired size of microstructures was prepared. This surface was then mounted on a Peltier cooler and brought to temperatures below the dew point for video observation (Video S1, Supporting Information). Two experiments were conducted: one with the bare SS mesh as a control and another with the sample, TiO_2 microstructure-coating. This allowed us to directly compare the efficiency of the fabricated material for atmospheric water capture. In both the experiments, the surface under examination was carefully attached to the Peltier cooler using silver paste to ensure efficient heat transfer. The entire setup was placed on the viewing stage of a Keyence VHX-950F digital microscope within a controlled environment maintained at 50% relative humidity and 25 °C temperature (dew point ≈13.8 °C). The surface was illuminated for clear microscopic observation. Time-lapse optical microscopy was performed to monitor the nucleation and growth of water droplets on the bare SS mesh and the TiO_2 microstructured surface under the above-mentioned laboratory conditions. There was no separate airflow to the substrate. The temperature of the condensing surface was 12 °C and it was measured using a thermocouple.

Photocatalytic Application Using the Microstructures. To examine the photocatalytic activity of ESD-fabricated TiO_2 micro-

https://doi.org/10.1021/acssuschemeng.4c02806
ACS Sustainable Chem. Eng. XXXX, XXX, XXX−XXX

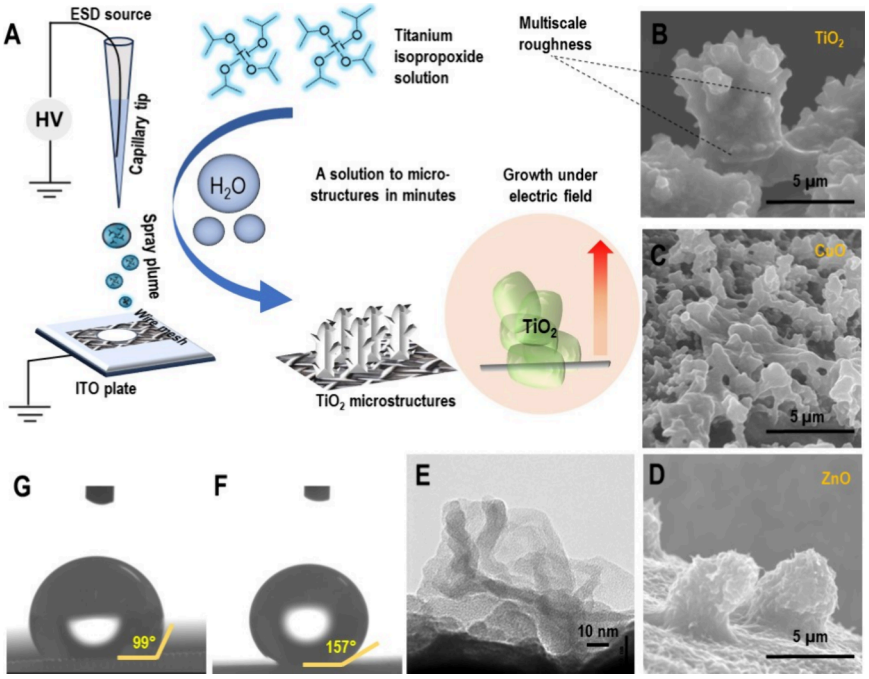

Figure 1. (A) Schematic representation of the ESD fabrication setup used for the microdroplet synthesis of microstructures under ambient conditions. SEM images of (B) TiO_2, (C) CuO and (D) ZnO microstructures. (E) TEM image of TiO_2 microstructure. Contact angle of water on (F) TiO_2 microstructures, and (G) normal SS wire mesh.

structures, degradation of recalcitrant molecules and dyes was studied using the surface. In all our photocatalytic experiments, natural sunlight was used as the light source, and the samples were exposed to direct sunlight for a specific duration. In the case of ibuprofen, the solution was prepared, and the microstructured surface was immersed in the solution for 30 min. Ibuprofen is a persistent anti-inflammatory drug. Following adsorption, the contaminated surface was exposed to sunlight for 3 h, followed by washing with the desired solvent for extraction of the degradation products for further analysis. Similarly, a mixture of rhodamine 6G, rhodamine B, and methylene blue dyes was prepared. The microstructured surface was then dipped in the solution, and the dried surface was kept under sunlight for 3 h, followed by optical photography.

Antibacterial Activity of the TiO_2 Microstructures. The antibacterial and antiadhesion properties of the TiO_2 microstructured surfaces were assessed using *Escherichia coli* MTCC 443. For all the experiments, fresh cultures of *E. coli* were prepared by reviving the glycerol stock culture stored at −80 °C in Luria−Bertani (LB) broth, followed by incubation at 37 °C with shaking at 120 rpm. The revived culture was then introduced into freshly prepared LB broth to achieve a concentration of 10^5 CFU/mL. For antiadhesion investigations, the cells were centrifuged at 3000 rpm and rinsed twice with 0.2 M sterile phosphate-buffered saline (PBS, pH 7.5). Subsequently, the cells were suspended in sterile PBS and applied onto various surfaces: a bare SS wire mesh (sample 1), a SS wire mesh coated with TTIP (5 mM) (sample 2), and a TiO_2 microstructured surface (sample 3). After 1 h interaction period with the surfaces at 37 °C, they were rinsed with sterilized PBS to eliminate unadhered cells. The samples were then shaken at 100 rpm in sterile PBS for 1 h to collect the adhered cells. Colony counting was employed to determine the number of cells adhered to the surfaces by inoculating the collected cells onto freshly prepared nutrient agar (NA) plates, followed by incubation at 37 °C for 24 h.

The resistance to bacterial proliferation was examined by incubating *E. coli* culture at a concentration of 10^3 CFU/mL in LB broth on the surfaces at 37 °C for 1 day with gentle agitation. The surfaces were subsequently rinsed with PBS to remove suspended and unadhered cells. The cells grown on the surfaces were retrieved with PBS through gentle agitation for 1 h. This cell suspension was then plated onto NA plates and incubated under standard conditions, followed by colony counting. The antibacterial efficacy against *E. coli* was evaluated by loading the surfaces with a bacterial suspension of 10^4 CFU/mL and allowing interaction for 1 h under sunlight in static conditions. Control samples were kept in darkness to assess the influence of sunlight. The bacterial suspension on the wire mesh was collected by successive washings with PBS and plated onto freshly prepared NA plates for colony counting after 24 h of incubation at 37 °C. Live/dead staining was performed using the BaclightTM Live/Dead viability kit, with a stain prepared by mixing SYTO 9 and propidium iodide dyes in PBS in a 1:1 ratio to visualize the *E. coli* cells under a fluorescence microscope.

The suitability of the TiO_2 coating as an antibacterial surface over repeated cycles of bacterial exposure was investigated to assess its longevity. This involved repeating the antibacterial studies for 5 cycles on the same sample surface. All experiments were conducted in triplicate for each sample.

RESULTS AND DISCUSSION

From Solution to Microstructures. Figure 1A presents a schematic diagram of the custom-built nESI source employed for ESD to make the TiO_2 microstructures. The left-hand portion of the figure illustrates the electrical connections, the nESI tip, and the platinum wire facilitating contact with the precursor solution. TTIP ($C_{12}H_{28}O_4Ti$), readily available as an inorganic complex, served as the precursor for constructing the TiO_2 microstructures. This complex readily dissolves in polar solvents like ethanol (EtOH) and isopropyl alcohol (IPA) but undergoes instant hydrolysis and condensation to form TiO_2 in the presence of water. Therefore, utilizing pure and anhydrous solvents is crucial for our experiments. Otherwise, TTIP reacts with even trace amounts of moisture present in the solvent, leading to premature formation of TiO_2 and clogging of the nESI tip. Initial ESD experiments were conducted using a 10 mM solution of TTIP in EtOH. Later we reduced the concentration of TTIP, using 5 mM solution for all the experiments. A clear precursor solution was loaded into a ∼30 μm nESI tip and connected to the electrospray source. High voltage (1.5−2 kV)

https://doi.org/10.1021/acssuschemeng.4c02806
ACS Sustainable Chem. Eng. XXXX, XXX, XXX−XXX

was applied to the solution formed a Taylor cone, followed by a stable spray of charged microdroplets containing dissolved precursor ions. These droplets were directed toward a SS wire mesh as described in the experimental section. As deposition progressed, a white spot gradually grew in diameter, becoming more prominent with longer deposition times. This spot was characterized using electron microscopy, revealing pillar-like structures upon closer inspection. Figure 1B showcases an FESEM image of one such pillar formed after 90 min of deposition. Surprisingly, EDS analysis of the same pillar identified it as composed of TiO_2. Figure S1 presents the EDS spectrum, highlighting the atomic percentages of titanium and oxygen. The next paragraph delves deeper into the mystery, dissecting the surprising journey from a solution of $C_{12}H_{28}O_4Ti$ to TiO_2, within minutes, and its subsequent orientation to form the pillars with dimensions of tens of micrometers.

Based on the ion evaporation model (IEM) of electrospray, we know that the molecules within charged microdroplets exhibit a tendency to migrate toward the droplet's periphery.[63] We hypothesize that this behavior plays a crucial role in our microstructure formation. The high propensity of TTIP to undergo hydrolysis and form TiO_2 combined with the IEM forms the foundation of this process. We propose the following sequence of events during the flight path of the charged droplets:

1. As the charged microdroplets travel through air, TTIP molecules migrate toward the periphery of the droplet sphere.
2. These TTIP molecules at the periphery react with atmospheric moisture, forming TiO_2.

This process is schematically depicted in Figure 1A. Beyond converting the precursor to TiO_2, the arrangement of these molecules into microscale structures is paramount to the fabrication process (Figure 1A, bottom portion). First, powerful electrostatic forces act as the driving force, helping the assembly. Second, charged microdroplets containing TiO_2 particles and solvated ions of the unreacted portion of the precursor are deposited on the surface. Subsequent solvent evaporation induces spatial reorganization, leaving behind neutralized TiO_2 deposits contributing to the pillar-like structure. Finally, the observed rough edges can be attributed to two factors: head-on accumulation of incoming material and their orthogonal association, leading to the formation of pillars. The SS wire mesh plays a crucial role in this process. The applied potential difference generates a strong electric field within the gap of the wire mesh, guiding the incoming microdroplets. This field, calculated as 1.5×10^5 V/m for a 1500 V potential difference, effectively attracts and "harpoons" the charged microdroplets into the high-field region near the mesh. Here, they are deposited and neutralized. The deposited TiO_2 particles, now in the nanometre range, significantly alters the electric field experienced by the incoming microdroplets. To test this hypothesis, we conducted a control experiment with a 2 min fixed deposition time, followed by TEM imaging of the sample. Figure S2 shows a TEM image of a TiO_2 structure formed on the TEM grid, with its dimensions in the range of 20−30 nm. The field strength is calculated to be 1.89×10^{11} V/m for a 10 nm particle attached to the mesh. This enhanced field, radiating outward from the deposited particles, creates a strong, attractive force for the next set of charged microdroplets, driven by the Coulombic interaction. Notably, at these elevated fields, especially after initial growth, field emission may play a role in droplet neutralization. Furthermore, the deposited material itself becomes a point of even higher electric field, further attracting and guiding the assembly of incoming microdroplets, ultimately promoting the growth of elongated microstructures. The SS wire mesh is essential to create the structures. In its absence, on a standard ITO plate as substrate, the elongated microstructure was not seen (Figure S3).

Characterization of the Microstructures and Their Superhydrophobic Property. TEM was performed on the fabricated TiO_2 microstructures to investigate their crystalline nature. For this, ESD was performed on a copper TEM grid without carbon coating. Figure 1E shows a TEM image of a representative TiO_2 pillar. A closer investigation revealed that these pillars are made of amorphous TiO_2. Following an investigation of individual TiO_2 micropillars, their collective behavior as a surface was assessed. Notably, despite the intrinsic hydrophilicity of TiO_2, exhibited by its widespread utilization as a hydrophilic coating material, the surface fabricated via ESD unexpectedly displayed superhydrophobic characteristics. This phenomenon is particularly intriguing as the collective architecture of the micropillars seemingly negates the inherent hydrophilicity of the individual components, resulting in a surface with a significantly higher water contact angle (157°, Figure 1F) compared to a standard stainless-steel mesh (99°, Figure 1G). The reason behind the superhydrophobic character of the surface can be attributed to the following two reasons: (i) Air trapping: microstructures trap air pockets between the consecutive pillars. These air pockets create a barrier between the water and the solid surface, minimizing the direct contact area and reducing the attractive forces between water molecules and the surface.[64] (ii) Hierarchical Texture: ESD fabricated TiO_2 surfaces exhibit multiscale roughness, as evident from the FESEM image shown in Figure 1B, where each pillar has microstructures with even smaller features within. This hierarchical texture amplifies air trapping and contact angle effects, leading to even stronger hydrophobicity.[65] Water droplet roll-off experiments were carried out on the TiO_2 microstructures as well as on the SS mesh and the data were captured using a Keyence microscope (Figures S4 and S5).

Extending the Methodology to Other Metal Oxides. We tested the feasibility of generalizing this methodology for the fabrication of microstructures for multiple metal oxides. Figures 1C and 1D show FESEM images of microstructures created from ESD deposition of copper(II) acetate monohydrate ($Cu(CO_2CH_3)_2{\cdot}H_2O$), and zinc acetate dihydrate ($Zn(CH_3COO)_2{\cdot}2H_2O$). Ethanolic solutions of 5 mM concentration each were used for ESD. We used ethanolic solutions instead of aqueous solutions for our experiments due to significantly faster electrospray times. This difference was primarily attributed to the solvents' surface tension. Ethanol, with its lower surface tension (21.6 mN/m at 20 °C compared to 72.8 mN/m for water), allows for easier droplet formation and faster electrospray, significantly reducing the fabrication time. Figure S6 shows the large area FESEM images of the fabricated surface, proving that it can be created over a significantly large area. EDS analysis confirms the microstructures' composition, identifying them as CuO (Figure S6A) and ZnO (Figure S6B), respectively. Both surfaces, made of copper and zinc oxide, showed hydrophobic properties when tested. Our findings extend the reach of ambient ESD beyond typical materials, demonstrating its prowess in fabricating superhydrophobic microstructures of vastly different metal oxides. The contact angle measurements of the CuO and ZnO microstructures were

https://doi.org/10.1021/acssuschemeng.4c02806
ACS Sustainable Chem. Eng. XXXX, XXX, XXX−XXX

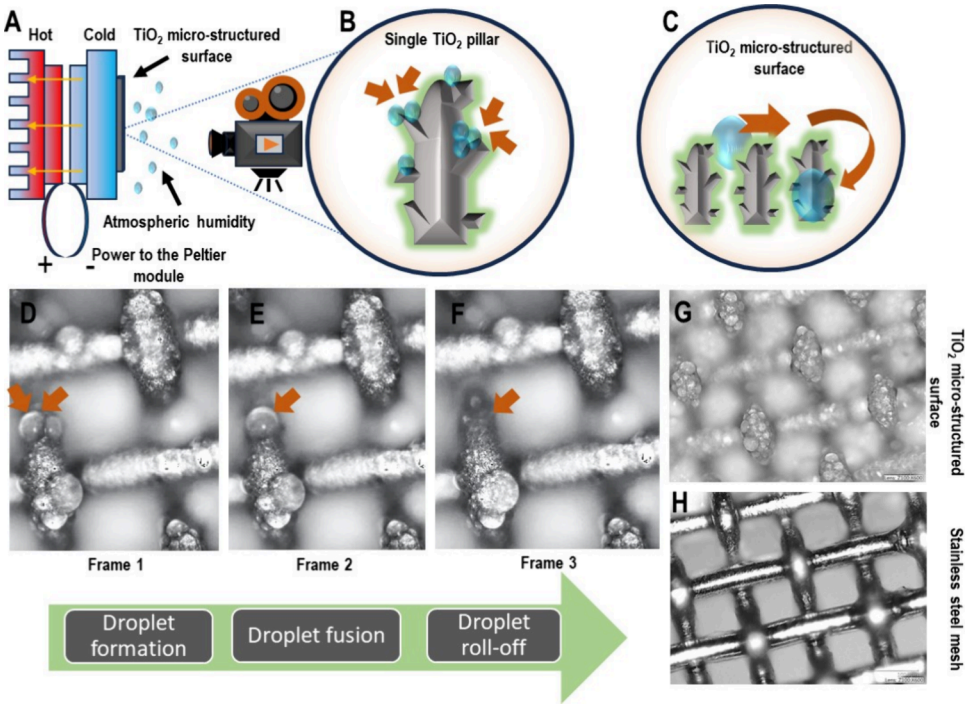

Figure 2. (A) Experimental setup for water harvesting. Schematic representation of (B) droplet formation, and (C) droplet roll-off on a single TiO_2 microstructure. Microscopic image of water harvesting, where the red arrow indicates the successive events of (D) droplet formation, (E) droplet fusion, and (F) droplet roll-off, on TiO_2 microstructures. Comparison between water harvesting efficiency of (G) TiO_2 microstructured surface and (H) stainless steel mesh, upon exposure to the environment, keeping all parameters the same. Details of the experiment are presented in the main text.

157° (Figure S7). This versatility paves the way for exploring a rich materials landscape.

Controlling Parameters for the Dimensions of the Microstructures. The size, shape, and performance of the fabricated microstructures can be finely tuned by adjusting specific parameters within the ESD process. However, maintaining certain parameters is critical for ensuring the generation of reproducible hydrophobic surfaces. This section describes the key fabrication parameters and their influence on the final product.

Deposition Time. The impact of deposition time was investigated by varying the ESD duration from 30 min to 2 h (Figure S8). FESEM images reveal a clear trend; longer deposition times leading to taller vertically growing structures.

Deposition Rate. To optimize microstructure morphology, the ESD deposition rate was monitored via measurements of the deposition current. A current range of 10−12 nA produced ideal microstructures with sharp, multilayered edges. Higher currents resulted in increased deposition of unreacted precursors, leading to rounded edges and significantly reduced water repellency (Figure S9). This highlights the importance of controlling the deposition rate for achieving optimal surface wettability.

Tip Size. For ESD fabrication of TiO_2 microstructures, tip size plays a crucial role in ensuring smooth process flow and minimizing unreacted precursors. All the experiments were performed using the tip size of 25−30 μm. The size of each tip was measured using an optical microscope before proceeding with the ESD process. Figure S10 shows a representative optical image of one such tip. Any tip that did not match the optimum size window was discarded.

Distance between the Spray Tip and the SS Wire Mesh. Electrostatic field strength, governed by the distance between the spray tip and the SS wire mesh, is a critical factor influencing the stacking of the incoming droplets. To achieve uniform microstructures, we optimized this distance to 8−10 mm. While a closer distance would generate a stronger field, it could lead to inadequate solvent evaporation, creating solvent bridges that disrupt the fabrication process.

Atmospheric Water Capture Using TiO_2 Microstructures. Unexpected transformation of an intrinsically hydrophilic material into a superhydrophobic one, achieved through ESD prompted us to explore its possible use in atmospheric water capture (AWC). This interest stemmed from a biomimetic perspective; nature provides numerous examples of highly efficient AWC strategies often relying on intricate hydrophilic−hydrophobic surface patterns.[51,66] A prime example is the *Opuntia microdasys*, where minute barbs on its conical spines effectively condense water droplets, while the spine's curvature acts as a natural microfluidic channel, guiding the condensate toward the base through a combination of hydrophilic and hydrophobic regions.[67] On the other hand, the Namib desert beetle (*Stenocara gracilipes*) utilizes hydrophilic−hydrophobic patterns on its wings to both collect water and, subsequently, transport it to other parts of its body.[51] These observations served as a strong motivator to explore the AWC potential of our ESD-fabricated superhydrophobic surface. For our experiments, a ∼ 100 mm^2 circular area of TiO_2 microstructures, fabricated via ESD on a 1 cm^2 stainless steel mesh, served as the AWC surface. This mesh was secured onto a Peltier cooler using silver paste for efficient thermal contact. AWC experiments were conducted in an air-conditioned room (∼25 °C, 50% RH) with the surface temperature maintained at 10 °C, slightly below the dew point (13.8 °C). No external humidifiers or mist generators were employed. The collection surface and cooling module were positioned vertically on a Keyence microscope stage for video recording. Figure 2A schematically illustrates the experimental

https://doi.org/10.1021/acssuschemeng.4c02806
ACS Sustainable Chem. Eng. XXXX, XXX, XXX−XXX

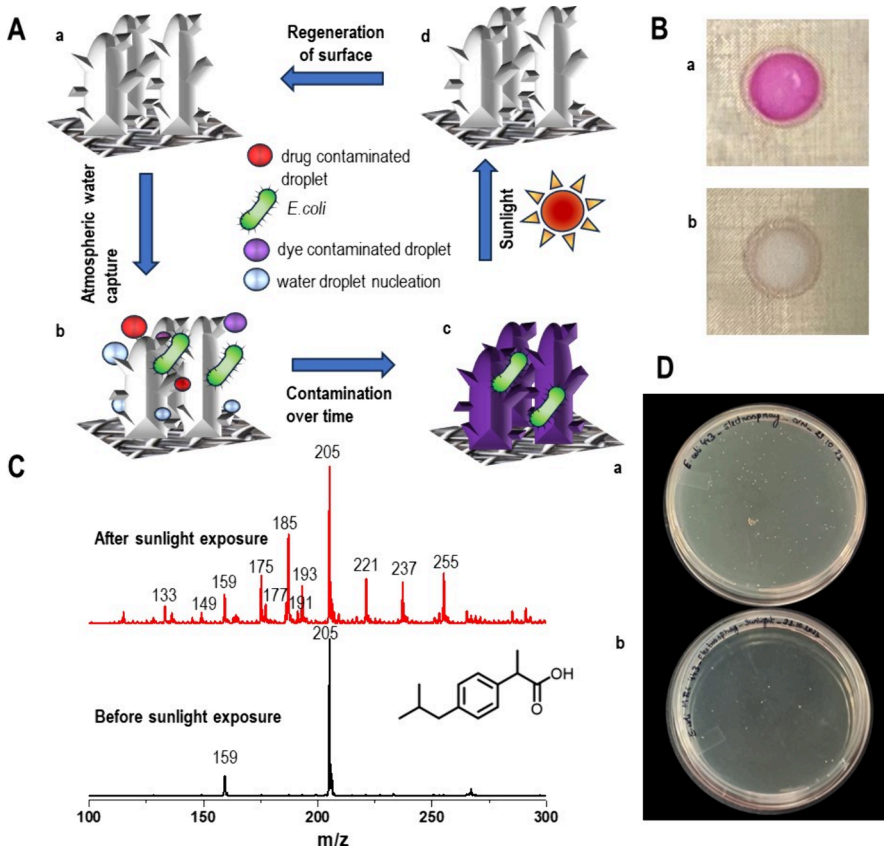

Figure 3. (A) Schematic representation of atmospheric water capture and self-cleaning property of TiO_2 microstructures: (a) TiO_2 microstructures; (b) TiO_2 microstructures during atmospheric water harvesting; (c) contaminated microstructures over time; (d) regenerated TiO_2 microstructures upon sunlight exposure. (B) Optical images of the TiO_2 microstructure surface on a SS wire mesh (a) after dye adsorption and (b) after sunlight exposure. (C) Mass spectra of ibuprofen collected from the solution after washing the drug-adsorbed TiO_2; the black and red traces are before and after sunlight exposure. (D) Optical images of *E. coli* colonies on TiO_2 microstructures (a) before and (b) after sunlight exposure.

setup of AWC. Surfaces with varying microstructures created by ESD for 1, 1.5, and 2 h were investigated for their AWC performance (Figure S11). Notably, while all surfaces exhibited water nucleation, the 1.5 h fabricated surface demonstrated superior water roll-off, a crucial factor for efficient AWC. Therefore, this optimized surface was chosen for further experiments due to its enhanced water collection and release capabilities. The AWC process on the fabricated TiO_2 microstructures can be conceptualized in three key stages:

1. Nucleation: The intricate nanoscale edges of the intrinsically hydrophilic TiO_2 structures readily initiate water droplet formation due to their ability to lower the free energy barrier for nucleation. This function can be likened to the minute barbs on a cactus spine, promoting water droplet condensation on the surface.

2. Coalescence: Once nucleated droplets reach a critical size, they begin to coalesce with each other due to intermolecular forces, forming larger and heavier droplets.

3. Roll-off: When the combined weight of a coalesced droplet overcomes the pinning force exerted by the underlying surface texture and exceeds the adhesive forces, the superhydrophobic nature of the microstructured surface facilitates its effortless roll off. This can be envisioned as a "critical weight threshold" being surpassed, triggered by the combined effect of superhydrophobicity and gravity.

Figures 2B and 2C schematically illustrate the three stages of the AWC process. Figures 2D-F present corresponding optical images, captured from video recordings from the microscope, showcasing a specific region (indicated by the red arrow) where all three stages (nucleation, coalescence, and roll-off) can be sequentially observed. For a dynamic visualization, please refer to Supporting Video S1, which presents a real-time video recording of the AWC process. To elucidate the role of the TiO_2 microstructures in water nucleation, a control experiment was performed using a bare stainless-steel mesh under identical AWC conditions. As evident from Figures 2G and 2H, the TiO_2 microstructured surface exhibited significantly enhanced water nucleation compared to the minimal condensation observed on the bare mesh. Figure S12 shows FESEM images of the surface after keeping the surface underwater for 1 h.

The AWC efficiency for the TiO_2 microstructures (created by 90 min of deposition) was calculated based on the droplets generated on a measured area within a fixed time (90 s). Figure S13 shows the reference image used for the efficiency calculation. From this image, a rectangular area measuring 130.3 μm in length and 34.1 μm in width was selected, and the number of droplets within this area (seven, in this case) was counted, indicated by black crosses in Figure S13. The diameter of a single droplet was then measured; a smaller droplet with a diameter of 17.7 μm was chosen to avoid overestimation. Larger droplets were intentionally excluded from consideration as they resulted from the coalescence of smaller droplets. The volume of water in each droplet was calculated, assuming it to be a

https://doi.org/10.1021/acssuschemeng.4c02806
ACS Sustainable Chem. Eng. XXXX, XXX, XXX−XXX

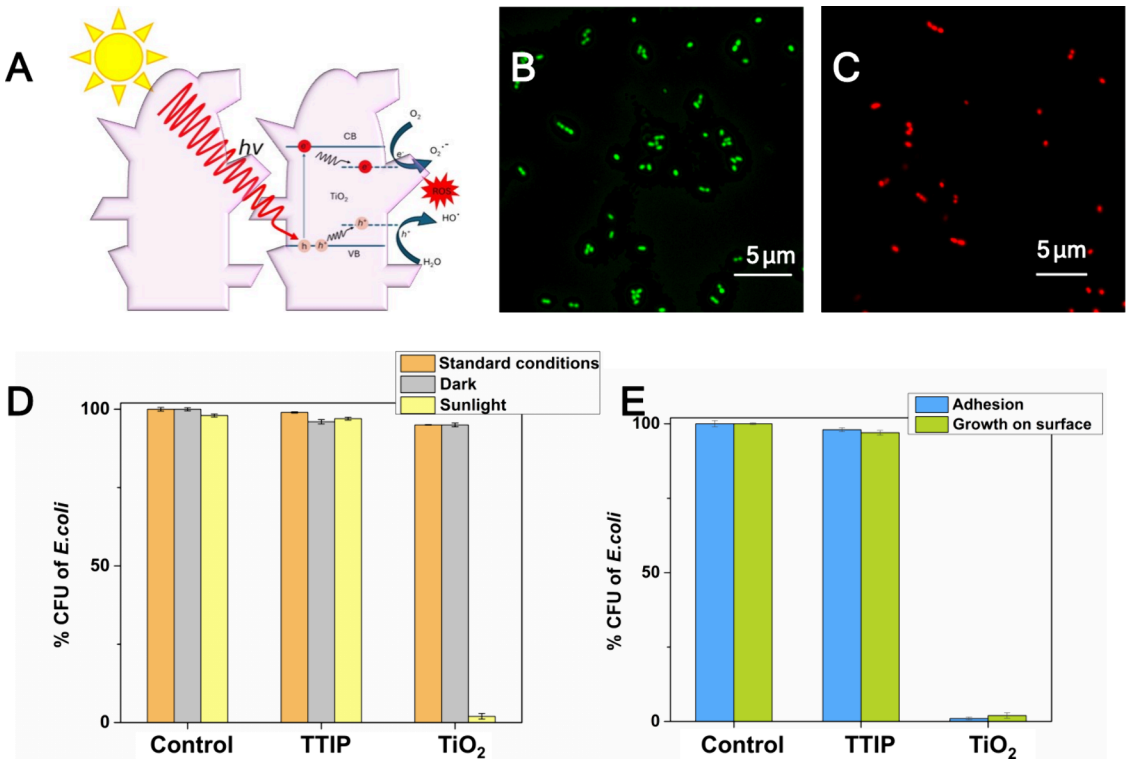

Figure 4. (A) Schematic representation of the mechanism of ROS formation on the microstructures due to photocatalytic activation of TiO_2. Fluorescence microscopy image of (B) *E. coli* control cells and (C) cells exposed to sunlight on TiO_2 surface. (D) Viability of *E. coli* cells on SS mesh, TTIP drop casted surface, and TiO_2 microstructure; experiments were done under standard conditions in the dark as well as in the presence of sunlight. (E) Bar diagram shows the reduction in the growth and adhesion in the *E. coli* cells exposed to TiO_2 surface compared with control cells and TTIP.

hemisphere. This process was repeated in several other areas, and the values were averaged and converted into units of L m^{-2} day^{-1}. We estimate that the TiO_2 microstructured surface demonstrated a water capture efficiency of ~40 L m^{-2} day^{-1}.

Photocatalytic Self-Cleaning of TiO_2 Microstructures for Prolonged AWC. Degradation of Organic Molecules. Figure 3A schematically illustrates self-cleaning mechanism of the fabricated TiO_2 microstructures. Initially, the clean surface captures atmospheric water vapor (3Aa, 3Ab), leading to potential contamination due to the different contaminants present in the atmosphere. But in our case, the sunlight exposure triggers a regenerative process (3Ad) because of the photocatalytic activity of TiO_2. To assess this self-cleaning capability, photocatalytic degradation of various pollutants was investigated. A mixture of dyes (rhodamine 6G, rhodamine B, methylene blue) was adsorbed onto the surface and exposed to sunlight for 3 h. Remarkably, no visible trace of dye remained (Figures 3Ba, 3Bb show before and after sunlight exposure, respectively), highlighting the effectiveness of TiO_2 microstructures for both self-cleaning and degrading diverse organic pollutants. Similarly, ibuprofen served as a model drug to test the effect. A 10 mM solution (1:9 methanol: water) was prepared and the microstructure surface was immersed for 30 min. Following adsorption, the surface was exposed to sunlight for 3 h. Subsequent washing and mass spectrometry analysis revealed significant degradation of ibuprofen (Figures 3C and S14, the black and red traces demonstrate before and after sunlight exposure). The decrease in the intensity of m/z 205 peak suggests breakdown via the OH radical-induced pathway, further evidenced by the appearance of additional peaks signifying the addition of OH groups (m/z 221, 237, 255 (H_2O adduct of m/z 237)). The peaks at lower mass ranges are peaks due to further degradation of the hydroxylated products. The degradation products and corresponding m/z values are mentioned in the Table S1. Although these peaks may be attributed to species of higher toxicity than the parent molecules, they are short-lived intermediates of the entire degradation pathway and the final degradation product may be harmless. Control experiments proved that in the absence of TiO_2 there was no degradation of the drug molecule. TiO_2 typically has a large band gap (>3.2 eV), which means it can only absorb UV light and not visible light, limiting its photocatalytic activity under sunlight. However, we speculate that the following factors may have contributed to the photocatalytic activity of the TiO_2 microstructures under sunlight. Size and surface area: The microstructures created using ambient microdroplet deposition had a high surface area-to-volume ratio, which increased the availability of active sites for photocatalytic reactions.[68,69] Enhanced light absorption: The curvatures and micronanometre-sized grooves (evident from Figure 1B) of microstructures led to light scattering and multiple reflections within the structures, enhancing the absorption of sunlight, including the UV component. Doping and defects: As mentioned previously, the synthesized TiO_2 was amorphous, implying it may have oxygen defects.[70] Oxygen defects are common in amorphous materials due to their lack of long-range crystalline order. These oxygen vacancies create defect states within the band gap, effectively reducing the band gap energy. This reduction probably allowed the TiO_2 microstructures to absorb visible light, extending its photocatalytic activity beyond the UV region. Increased surface reactivity: The presence of oxygen defects increased the number of active sites on the surface of amorphous TiO_2. These active sites facilitated the adsorption

https://doi.org/10.1021/acssuschemeng.4c02806
ACS Sustainable Chem. Eng. XXXX, XXX, XXX−XXX

and activation of reactant molecules, leading to higher photocatalytic activity.

Antibacterial Property of the TiO_2 Microstructures. Water harvesting surfaces face challenges posed by bacterial growth, impacting long-term efficacy. This study assessed the antibacterial activity of ESD-fabricated TiO_2 microstructures under sunlight using *E. coli* bacteria. Significant bacterial killing was observed on sunlight -exposed TiO_2 sample (Figure 3Db), contrasting with the absence of such activity in the samples maintained in the dark (Figure 3Da). Control experiments (Figure S15A) with blank wire mesh and TTIP coated (by drop casting method) mesh under light and dark conditions reinforced these findings. This confirms the effectiveness of sunlight-exposed TiO_2 surfaces in eliminating bacteria.

Literature provides a framework for understanding the degradation and antibacterial properties of TiO_2.[71] Under sunlight, the TiO_2 microstructure undergoes photoexcitation. An electron leaps from the valence band (VB) to the conduction band (CB), creating a hole in the VB. These energetic electron−hole pairs migrate to the surface. Here, they interact with adsorbed water and oxygen, generating highly reactive oxygen species (ROS) like hydroxyl radicals ($^{\bullet}OH$) and superoxide radicals ($O_2^{\bullet-}$). Figure 4A schematically represents the mechanism of ROS generation on the TiO_2 microstructures upon photoexcitation. Ultimately, the generated ROS are responsible for the degradation and antibacterial properties of TiO_2.

Previous studies have established the enhanced antibacterial properties of TiO_2 under sunlight. Subsequent experiments were conducted to test and quantify the antibacterial efficacy of the ESD-fabricated surfaces. Fluorescence imaging of *E. coli* cells was carried out to assess antibacterial activity. Figure 4B presents a fluorescence image of *E. coli* cells drop-casted on a SS wire mesh and exposed to sunlight. The presence of green emission indicates live bacterial cells in the absence of TiO_2. Conversely, Figure 4C shows cells after exposure to sunlight with TiO_2 microstructures. The red-stained cells indicate dead bacteria proving the antibacterial effect of TiO_2.[72] Evaluation of the antibacterial activity revealed a viability of 2% in bacterial cells exposed to sunlight with TiO_2 compared to 97% in cells treated with TTIP and the control group (refer to Figure 4D). Control experiments were conducted under standard conditions and in the absence of sunlight to confirm the role of TiO_2 structures in *E. coli* eradication. The antibacterial efficacy of TiO_2 persisted even after subjecting it to five cycles of loading with 10^4 CFU/mL of *E. coli* cells and exposure to sunlight (refer to Figure S15B). This was contrasted with bacterial cells incubated on wire mesh kept in the dark and another control group exposed to sunlight. The high antibacterial activity may also be attributed to the surface roughness of the microstructures. Literature suggests that nanometer-scale structures with high aspect ratios do not facilitate the growth of *E. coli* cells.[73]

The presence of a hydrophobic surface significantly hampered *E. coli* growth, with only 2% of viable cells detected after 24 h of incubation under standard conditions. In contrast, drop casted surfaces facilitated bacterial growth and exhibited adherence. Notably, TiO_2 surfaces demonstrated notable resistance to bacterial attachment, attributed to their high hydrophobicity and ROS production, showcasing their efficacy in inhibiting bacterial biofilm formation.

The self-cleaning property was evaluated using *E. coli* cells, where TiO_2 surfaces loaded with these cells were subjected to gentle washing. Colony counting on nutrient agar plates revealed that TiO_2 microstructures effectively deterred *E. coli* adhesion in water, with only 1% adherence observed, contrasting starkly with wire mesh, which retained 98% of bacterial cells postwashing (refer to Figure 4E).

Sustainability of the ESD Technique. Creation of nanomicro structures on surfaces using conventional techniques like, electron lithography, chemical vapor deposition, physical vapor deposition, cathodic arc deposition, magnetron sputtering, etc., requires specific conditions like, high-temperature, high-vacuum, definite gas environments, etc. These requirements eventually add up to the carbon footprint of the synthesis method. In contrast, ESD serves as a sustainable solution by promoting direct conversion of a precursor solution to microstructures by a feasible room-temperature technique with minimal use of chemicals and energy. In this report, we present a technique that converts TTIP, a precursor solution of Ti to TiO_2 microstructures within minutes at room temperature. These microstructures can be utilized as a standalone surface for atmospheric water capture and treatment to address one of the sustainable development goals.

CONCLUSIONS

This study presents a novel, eco-friendly, and convenient method for producing extensive TiO_2 microstructures directly from a TTIP solution under ambient conditions. These specially designed microstructures, collectively offer great super hydrophobicity allowing water droplets to roll-off efficiently despite TiO_2's inherent hydrophilic nature, enabling efficient atmospheric water harvesting. Under sunlight, the photocatalytic properties of TiO_2 activate breaking down of contaminants like organic dyes and drugs, resulting in an essentially self-cleaning surface for sustainable water collection. Sunlight also generates ROS that prevent bacterial growth and biofilm formation, addressing a key challenge for long-term use. This unique combined capability allows for the independent collection and purification of water from the atmosphere, offering a promising solution for water scarcity challenges. Additionally, the approach's versatility was demonstrated by successfully creating microstructures from other metal oxide solutions, highlighting its potential for broader applications.

ASSOCIATED CONTENT

Supporting Information

The Supporting Information is available free of charge at https://pubs.acs.org/doi/10.1021/acssuschemeng.4c02806.

Video S1 of water capture in TiO_2 microstructure (MP4)

FESEM image and EDS spectra of TiO_2 microstructures; TEM image of TiO_2 structure formed after 2 min of deposition; FESEM image of deposited TiO_2 on an ITO plate; a water droplet roll-off experiment on TiO_2 microstructure surface; a water droplet adhesion experiment on TiO_2 microstructures and SS wire mesh; FESEM images and EDS spectra of CuO and ZnO microstructures; contact angles of CuO-coated SS mesh and ZnO-coated mesh; time-dependent FESEM images of TiO_2 microstructures; FESEM image of TiO_2 structures at higher deposition rate; optical image of a nESI tip; atmospheric water harvesting on TiO_2 microstructures; FESEM of surface immersed in water; optical image of TiO_2 microstructures during the AWC experiment; mass spectrum for ibuprofen degradation; bacterial activity;

https://doi.org/10.1021/acssuschemeng.4c02806
ACS Sustainable Chem. Eng. XXXX, XXX, XXX−XXX

ibuprofen degradation products and m/z of the corresponding ions (PDF)

AUTHOR INFORMATION

Corresponding Authors

Depanjan Sarkar − *DST Unit of Nanoscience and Thematic Unit of Excellence, Department of Chemistry, Indian Institute of Technology Madras, Chennai 600036, India; Centre of Excellence on Molecular Materials and Functions, Department of Chemistry, Indian Institute of Technology Madras, Chennai 600036, India; International Centre for Clean Water, Indian Institute of Technology Madras Research Park, Chennai 600013, India*; Email: depanjansarkar@gmail.com

Thalappil Pradeep − *DST Unit of Nanoscience and Thematic Unit of Excellence, Department of Chemistry, Indian Institute of Technology Madras, Chennai 600036, India; Centre of Excellence on Molecular Materials and Functions, Department of Chemistry, Indian Institute of Technology Madras, Chennai 600036, India; International Centre for Clean Water, Indian Institute of Technology Madras Research Park, Chennai 600013, India*; orcid.org/0000-0003-3174-534X; Email: pradeep@iitm.ac.in

Authors

Keerthana Unni − *DST Unit of Nanoscience and Thematic Unit of Excellence, Department of Chemistry, Indian Institute of Technology Madras, Chennai 600036, India; Centre of Excellence on Molecular Materials and Functions, Department of Chemistry, Indian Institute of Technology Madras, Chennai 600036, India; International Centre for Clean Water, Indian Institute of Technology Madras Research Park, Chennai 600013, India*

Jenifer Shantha Kumar − *DST Unit of Nanoscience and Thematic Unit of Excellence, Department of Chemistry, Indian Institute of Technology Madras, Chennai 600036, India; Centre of Excellence on Molecular Materials and Functions, Department of Chemistry, Indian Institute of Technology Madras, Chennai 600036, India; International Centre for Clean Water, Indian Institute of Technology Madras Research Park, Chennai 600013, India*; orcid.org/0009-0003-7502-7005

Anirban Som − *DST Unit of Nanoscience and Thematic Unit of Excellence, Department of Chemistry, Indian Institute of Technology Madras, Chennai 600036, India; Centre of Excellence on Molecular Materials and Functions, Department of Chemistry, Indian Institute of Technology Madras, Chennai 600036, India; International Centre for Clean Water, Indian Institute of Technology Madras Research Park, Chennai 600013, India*; orcid.org/0000-0002-6646-679X

Complete contact information is available at: https://pubs.acs.org/10.1021/acssuschemeng.4c02806

Author Contributions

K.U.: design of the work, data collection, data analysis and interpretation, drafting and editing of the article. J.S.K.: microbiology and fluorescence microscopy experiments. A.S.: TEM measurements, data analysis, and interpretation. D.S.: conception and design of work, supervision of data analysis, interpretation of results, drafting and editing of the article. T.P.: conception and design of work, supervision of data analysis, interpretation of results, and writing of the final version of the article.

Notes

The authors declare no competing financial interest.

ACKNOWLEDGMENTS

We acknowledge the Science and Engineering Research Board (SERB), Department of Science and Technology (DST), and the Government of India for their research funding. T.P. acknowledges the financial support of SERB SUPRA (Grant SPR/2021/000439). D.S. acknowledges the Centre of Excellence on Molecular Materials and Functions under the Institution of Eminence Scheme of IIT Madras. K.U. thanks the University Grants Commission (UGC), Government of India, for her fellowship. J.S.K. thanks IIT Madras for research fellowship. We acknowledge Prof. Pijush Ghosh and Amit Kumar for helping us conduct the contact angle measurements.

ABBREVIATIONS

TTIP, titanium tetraisopropoxide; AWC, atmospheric water harvesting; VB, valence band; CB, conduction band; ROS, reactive oxygen species; ESD, electrospray deposition; SS, stainless steel; LB, Luria−Bertani; PBS, phosphate buffered saline; NA, nutrient agar; IPA, isopropyl alcohol; ITO, indium tin oxide

REFERENCES

(1) Wei, Z.; Li, Y.; Cooks, R. G.; Yan, X. Accelerated Reaction Kinetics in Microdroplets: Overview and Recent Developments. *Annu. Rev. Phys. Chem.* **2020**, *71* (1), 31−51.

(2) Girod, M.; Moyano, E.; Campbell, I.; Cooks, R. G. Accelerated Bimolecular Reactions in Microdroplets Studied by Desorption Electrospray Ionization Mass Spectrometry. *Chem. Sci.* **2011**, *2* (3), 501−510.

(3) Sahota, N.; AbuSalim, D. I.; Wang, M. L.; Brown, C. J.; Zhang, Z.; El-Baba, T. J.; Cook, S. P.; Clemmer, D. E. A Microdroplet-Accelerated Biginelli Reaction: Mechanisms and Separation of Isomers Using IMS-MS. *Chem. Sci.* **2019**, *10* (18), 4822−4827.

(4) Mehrgardi, M. A.; Mofidfar, M.; Zare, R. N. Sprayed Water Microdroplets Are Able to Generate Hydrogen Peroxide Spontaneously. *J. Am. Chem. Soc.* **2022**, *144* (17), 7606−7609.

(5) Lee, J. K.; Samanta, D.; Nam, H. G.; Zare, R. N. Micrometer-Sized Water Droplets Induce Spontaneous Reduction. *J. Am. Chem. Soc.* **2019**, *141* (27), 10585−10589.

(6) Meng, Y.; Gnanamani, E.; Zare, R. N. Catalyst-Free Decarboxylative Amination of Carboxylic Acids in Water Microdroplets. *J. Am. Chem. Soc.* **2023**, *145* (1), 32−36.

(7) Meng, Y.; Gnanamani, E.; Zare, R. N. One-Step Formation of Pharmaceuticals Having a Phenylacetic Acid Core Using Water Microdroplets. *J. Am. Chem. Soc.* **2023**, *145* (14), 7724−7728.

(8) Meng, Y.; Zare, R. N.; Gnanamani, E. One-Step, Catalyst-Free Formation of Phenol from Benzoic Acid Using Water Microdroplets. *J. Am. Chem. Soc.* **2023**, *145* (35), 19202−19206.

(9) Li, A.; Luo, Q.; Park, S. J.; Cooks, R. G. Synthesis and Catalytic Reactions of Nanoparticles Formed by Electrospray Ionization of Coinage Metals. *Angew. Chemie - Int. Ed.* **2014**, *53* (12), 3147−3150.

(10) Li, A.; Baird, Z.; Bag, S.; Sarkar, D.; Prabhath, A.; Pradeep, T.; Cooks, R. G. Cooks. Using Ambient Ion Beams to Write Nanostructured Patterns for Surface Enhanced Raman Spectroscopy. *Angew. Chem., Int. Ed.* **2014**, *53* (46), 12528−12531.

(11) Ghosh, J.; Cooks, R. G. Mass Spectrometry in Materials Synthesis. *TrAC - Trends Anal. Chem.* **2023**, *161*, No. 117010.

(12) Lee, J. K.; Samanta, D.; Nam, H. G.; Zare, R. N. Spontaneous Formation of Gold Nanostructures in Aqueous Microdroplets. *Nat. Commun.* **2018**, *9* (1), 1562.

(13) Sarkar, D.; Mahitha, M. K.; Som, A.; Li, A.; Wleklinski, M.; Cooks, R. G.; Pradeep, T. Metallic Nanobrushes Made Using Ambient Droplet Sprays. *Adv. Mater.* **2016**, *28* (11), 2223−2228.

(14) Fang, H.; Wang, D.; Yuan, L.; Wu, X.; Guo, H.; Chen, H.; Huang, K.; Feng, S. Electric-Field-Induced Assembly of Ag Nanoparticles on a CuO Nanowire Using Ambient Electrospray Ionization. *New J. Chem.* **2017**, *41* (8), 2878−2882.
(15) Sarkar, D.; Mondal, B.; Som, A.; Ravindran, S. J.; Jana, S. K.; Manju, C. K.; Pradeep, T. Holey MoS2 Nanosheets with Photocatalytic Metal Rich Edges by Ambient Electrospray Deposition for Solar Water Disinfection. *Glob. Challenges* **2018**, *2* (12), No. 1800052.
(16) Satyabola, D.; Ahuja, T.; Bose, S.; Mondal, B.; Srikrishnarka, P.; Kannan, M. P.; Spoorthi, B. K.; Pradeep, T. Transformation of Nanodiamonds to Onion-like Carbons by Ambient Electrospray Deposition. *J. Phys. Chem. C* **2021**, *125* (20), 10998−11006.
(17) Bose, S.; Chatterjee, A.; Jenifer, S. K.; Mondal, B.; Srikrishnarka, P.; Ghosh, D.; Chowdhuri, A. R.; Kannan, M. P.; Elchuri, S. V.; Pradeep, T. Molecular Materials through Microdroplets: Synthesis of Protein-Protected Luminescent Clusters of Noble Metals. *ACS Sustain. Chem. Eng.* **2021**, *9* (12), 4554−4563.
(18) Zhang, H.; Liu, Z.; Li, H.; Fu, Z.; Zhang, G.; Zhang, H.; Wang, G.; Zhang, Y. PdFe Alloy Nanoparticles Supported on Nitrogen- Doped Carbon Nanotubes for Electrocatalytic Upcycling of Poly(ethylene terephthalate) Plastics into Formate Coupled with Hydrogen Evolution. *J. Mater. Chem. A* **2024**, *12*, 15984−15995.
(19) Sarkar, D.; Mahapatra, A.; Som, A.; Kumar, R.; Nagar, A.; Baidya, A.; Pradeep, T. Patterned Nanobrush Nature Mimics with Unprecedented Water-Harvesting Efficiency. *Adv. Mater. Interfaces* **2018**, *5* (19), 1−7.
(20) Michalak, A. M.; Xia, J.; Brdjanovic, D.; Mbiyozo, A.-N.; Sedlak, D.; Pradeep, T.; Lall, U.; Rao, N.; Gupta, J. The Frontiers of Water and Sanitation. *Nat. Water* **2023**, *1* (1), 10−18.
(21) Williams, P.; Benton, L.; Warmerdam, J.; Sheehan, P. Comparative Risk Analysis of Six Volatile Organic Compounds in California Drinking Water. *Environ. Sci. Technol.* **2002**, *36* (22), 4721−4728.
(22) Ahuja, S. Overview: Current Status of Environmental Research on Water Contaminants. In *Contaminants in Our Water: Identification and Remediation Methods*; ACS Symposium Series, 1352; American Chemical Society, 2020; pp 1−11, DOI: 10.1021/bk-2020-1352.ch001.
(23) Wu, L.; Qiu, X.-W.; Wang, T.; Tao, K.; Bao, L.-J.; Zeng, E. Y. Water Quality and Organic Pollution with Health Risk Assessment in China: A Short Review. *ACS ES&T Water* **2022**, *2* (8), 1279−1288.
(24) Magnuson, M. L.; Allgeier, S. C.; Koch, B.; De Leon, R.; Hunsinger, R. Responding to Water Contamination Threats. *Environ. Sci. Technol.* **2005**, *39* (7), 153A−159A.
(25) Shah, A.; Arjunan, A.; Baroutaji, A.; Zakharova, J. A Review of Physicochemical and Biological Contaminants in Drinking Water and Their Impacts on Human Health. *Water Sci. Eng.* **2023**, *16* (4), 333−344.
(26) Schwarzenbach, R. P.; Egli, T.; Hofstetter, T. B.; von Gunten, U.; Wehrli, B. Global Water Pollution and Human Health. *Annu. Rev. Environ. Resour.* **2010**, *35* (1), 109−136.
(27) Lin, L.; Yang, H.; Xu, X. Effects of Water Pollution on Human Health and Disease Heterogeneity: A Review. *Front. Environ. Sci.* **2022**, *10*, 880246.
(28) Kumar, R.; Qureshi, M.; Vishwakarma, D. K.; Al-Ansari, N.; Kuriqi, A.; Elbeltagi, A.; Saraswat, A. A Review on Emerging Water Contaminants and the Application of Sustainable Removal Technologies. *Case Stud. Chem. Environ. Eng.* **2022**, *6*, No. 100219.
(29) Bashir, I.; Lone, F. A.; Bhat, R. A.; Mir, S. A.; Dar, Z. A.; Dar, S. A. Concerns and Threats of Contamination on Aquatic Ecosystems. *Bioremediation and Biotechnology: Sustainable Approaches to Pollution Degradation* **2020**, 1−26.
(30) Nagar, A.; Pradeep, T. Clean Water through Nanotechnology: Needs, Gaps, and Fulfillment. *ACS Nano* **2020**, *14* (6), 6420−6435.
(31) He, C.; Liu, Z.; Wu, J.; Pan, X.; Fang, Z.; Li, J.; Bryan, B. A. Future Global Urban Water Scarcity and Potential Solutions. *Nat. Commun.* **2021**, *12* (1), 1−11.
(32) Shemer, H.; Wald, S.; Semiat, R. Challenges and Solutions for Global Water Scarcity. *Membranes (Basel)* **2023**, *13* (6), 612.
(33) Reddy, S. M. W.; McDonald, R. I.; Maas, A. S.; Rogers, A.; Girvetz, E. H.; North, J.; Molnar, J.; Finley, T.; Leathers, G.; L. DiMuro, J. Finding Solutions to Water Scarcity: Incorporating Ecosystem Service Values into Business Planning at The Dow Chemical Company's Freeport, TX Facility. *Ecosyst. Serv.* **2015**, *12*, 94−107.
(34) Ahuja, S.. Overview of Global Water Challenges and Solutions. In *Water Challenges and Solutions on a Global Scale*; ACS Symposium Series, 1206; American Chemical Society, 2015; p 1, DOI: 10.1021/bk-2015-1206.ch001.
(35) Zhao, L.; Du, C.; Zhou, C.; Sun, S.; Jia, Y.; Yuan, J.; Song, G.; Zhou, X.; Zhao, Q.; Yang, S. Structurally Ordered AgNPs@C3N4/GO Membranes toward Solar-Driven Freshwater Generation. *ACS Sustain. Chem. Eng.* **2020**, *8* (11), 4362−4370.
(36) Kim, J. F.; Park, A.; Kim, S.-J.; Lee, P.; Cho, Y.; Park, H.; Nam, S.; Park, Y. Harnessing Clean Water from Power Plant Emissions Using Membrane Condenser Technology. *ACS Sustain. Chem. Eng.* **2018**, *6* (5), 6425−6433.
(37) Ndeketeya, A.; Dundu, M. Alternative Water Sources as a Pragmatic Approach to Improving Water Security. *Resour. Conserv. Recycl. Adv.* **2022**, *13*, No. 200071.
(38) Liu, X.; Beysens, D.; Bourouina, T. Water Harvesting from Air: Current Passive Approaches and Outlook. *ACS Mater. Lett.* **2022**, *4* (5), 1003−1024.
(39) Hu, Y.; Fang, Z.; Wan, X.; Ma, X.; Wang, Y.; Dong, M.; Ye, Z.; Peng, X. Ferrocene Dicarboxylic Acid Ligand-Exchanged Hollow MIL-101(Cr) Nanospheres for Solar-Driven Atmospheric Water Harvesting. *ACS Sustain. Chem. Eng.* **2022**, *10* (19), 6446−6455.
(40) Bagi, S.; Wright, A. M.; Oppenheim, J.; Dincă, M.; Román-Leshkov, Y. Accelerated Synthesis of a Ni2Cl2(BTDD) Metal−Organic Framework in a Continuous Flow Reactor for Atmospheric Water Capture. *ACS Sustain. Chem. Eng.* **2021**, *9* (11), 3996−4003.
(41) Wu, M.; Zhou, Y.; Aleid, S.; Tang, X.; Zhao, Y.; Li, R.; Wang, P. Recyclable and Degradable Biomass-Based Water Vapor Sorbents for Efficient Atmospheric Water Harvesting. *ACS Sustain. Chem. Eng.* **2024**, *12* (3), 1255−1264.
(42) Salehi, A. A.; Ghannadi-Maragheh, M.; Torab-Mostaedi, M.; Torkaman, R.; Asadollahzadeh, M. A Review on the Water-Energy Nexus for Drinking Water Production from Humid Air. *Renew. Sustain. Energy Rev.* **2020**, *120*, No. 109627.
(43) Ahrestani, Z.; Sadeghzadeh, S.; Motejadded Emrooz, H. B. An Overview of Atmospheric Water Harvesting Methods, the Inevitable Path of the Future in Water Supply. *RSC Adv.* **2023**, *13* (15), 10273−10307.
(44) Zhou, X.; Lu, H.; Zhao, F.; Yu, G. Atmospheric Water Harvesting: A Review of Material and Structural Designs. *ACS Mater. Lett.* **2020**, *2* (7), 671−684.
(45) Feng, A.; Akther, N.; Duan, X.; Peng, S.; Onggowarsito, C.; Mao, S.; Fu, Q.; Kolev, S. D. Recent Development of Atmospheric Water Harvesting Materials: A Review. *ACS Mater. Au* **2022**, *2* (5), 576−595.
(46) Wang, B.; Zhou, X.; Guo, Z.; Liu, W. Recent Advances in Atmosphere Water Harvesting: Design Principle, Materials, Devices, and Applications. *Nano Today* **2021**, *40*, No. 101283.
(47) Feng, A.; Mao, S.; Onggowarsito, C.; Naidu, G.; Li, W.; Fu, Q. Tillandsia-Inspired Composite Materials for Atmospheric Water Harvesting. *ACS Sustain. Chem. Eng.* **2023**, *11* (15), 5819−5825.
(48) Li, Z.; Tang, L.; Wang, H.; Singh, S. C.; Wei, X.; Yang, Z.; Guo, C. Nature-Inspired Surface Engineering for Efficient Atmospheric Water Harvesting. *ACS Sustain. Chem. Eng.* **2023**, *11* (30), 11019−11031.
(49) USGS. Atmosphere and the Water Cycle. 2019, https://www.usgs.gov/special-topics/water-science-school/science/atmosphere-and-water-cycle.
(50) Shi, Y.; Ilic, O.; Atwater, H. A.; Greer, J. R. All-Day Fresh Water Harvesting by Microstructured Hydrogel Membranes. *Nat. Commun.* **2021**, *12* (1), 2797.
(51) Zhang, F.; Guo, Z. Bioinspired Materials for Water-Harvesting: Focusing on Microstructure Designs and the Improvement of Sustainability. *Mater. Adv.* **2020**, *1* (8), 2592−2613.

(52) Zhang, Y.; Wang, T.; Wu, M.; Wei, W. Durable Superhydrophobic Surface with Hierarchical Microstructures for Efficient Water Collection. *Surf. Coat. Technol.* **2021**, *419*, No. 127279.
(53) Guo, Y.; Yu, G. Materials Innovation for Global Water Sustainability. *ACS Mater. Lett.* **2022**, *4* (4), 713−714.
(54) Zhang, S.; Huang, J.; Chen, Z.; Lai, Y. Bioinspired Special Wettability Surfaces: From Fundamental Research to Water Harvesting Applications. *Small* **2017**, *13* (3), No. 1602992.
(55) Lu, H.; Shi, W.; Guo, Y.; Guan, W.; Lei, C.; Yu, G. Materials Engineering for Atmospheric Water Harvesting: Progress and Perspectives. *Adv. Mater.* **2022**, *34* (12), No. 2110079.
(56) Chen, Y.; Zheng, Y. Bioinspired Micro-/Nanostructure Fibers with a Water Collecting Property. *Nanoscale* **2014**, *6* (14), 7703−7714.
(57) Zuo, Y.; Zheng, L.; Zhao, C.; Liu, H. Micro-/Nanostructured Interface for Liquid Manipulation and Its Applications. *Small* **2020**, *16* (9), No. 1903849.
(58) Ras, R. H. A.; Tian, X.; Chang, B.; Timonen, J. V. I. Droplet Manipulation on Liquid-Repellent Surfaces. In *Non-wettable Surfaces: Theory, Preparation, and Applications*; Ras, R. H. A., Marmur, A., Eds.; The Royal Society of Chemistry, 2016; pp 368−384; DOI: 10.1039/9781782623953-00368.
(59) Cao, M.; Ju, J.; Li, K.; Dou, S.; Liu, K.; Jiang, L. Facile and Large-Scale Fabrication of a Cactus-Inspired Continuous Fog Collector. *Adv. Funct. Mater.* **2014**, *24* (21), 3235−3240.
(60) Ghosh, R.; Baut, A.; Belleri, G.; Kappl, M.; Butt, H.-J.; Schutzius, T. M. Photocatalytically Reactive Surfaces for Simultaneous Water Harvesting and Treatment. *Nat. Sustain.* **2023**, *6* (12), 1663−1672.
(61) Wang, R.; Hashimoto, K.; Fujishima, A.; Chikuni, M.; Kojima, E.; Kitamura, A.; Shimohigoshi, M.; Watanabe, T. Light-Induced Amphiphilic Surfaces. *Nature* **1997**, *388*, 431−432.
(62) Fujishima, A.; Honda, K. Electrochemical Photolysis of Water at a Semiconductor Electrode. *Nature* **1972**, *238* (672), 37−38.
(63) Konermann, L.; Ahadi, E.; Rodriguez, A. D.; Vahidi, S. Unraveling the Mechanism of Electrospray Ionization. *Anal. Chem.* **2013**, *85* (1), 2−9.
(64) Parvate, S.; Dixit, P.; Chattopadhyay, S. Superhydrophobic Surfaces: Insights from Theory and Experiment. *J. Phys. Chem. B* **2020**, *124* (8), 1323−1360.
(65) Yoon, Y.; Kim, D.; Lee, J. B. Hierarchical Micro/Nano Structures for Super-Hydrophobic Surfaces and Super-Lyophobic Surface against Liquid Metal. *Micro Nano Syst. Lett.* **2014**, *2* (1), 1−18.
(66) Zhan, D.; Guo, Z. Overview of the Design of Bionic Fine Hierarchical Structures for Fog Collection. *Mater. Horizons* **2023**, *10* (11), 4827−4856.
(67) Gurera, D.; Bhushan, B. Passive Water Harvesting by Desert Plants and Animals: Lessons from Nature. *Philos. Trans. R. Soc. A Math. Phys. Eng. Sci.* **2020**, *378* (2167), 20190444.
(68) Zhao, T.; Zhao, Y.; Jiang, L. Nano-/microstructure improved photocatalytic activities of semiconductors. *Philosophical Transactions of the Royal Society A: Mathematical, Physical and Engineering Sciences* **2013**, *371* (2000), No. 20120303.
(69) Kamat, P. V. TiO_2 Nanostructures: Recent Physical Chemistry Advances. *J. Phys. Chem. C* **2012**, *116* (22), 11849−11851.
(70) Pham, H. H.; Wang, L. W. Oxygen Vacancy and Hole Conduction in Amorphous TiO_2. *Phys. Chem. Chem. Phys.* **2015**, *17* (1), 541−550.
(71) Yu, J. C.; Ho, W.; Lin, J.; Yip, H.; Wong, P. K. Photocatalytic Activity, Antibacterial Effect, and Photoinduced Hydrophilicity of TiO_2 Films Coated on a Stainless Steel Substrate. *Environ. Sci. Technol.* **2003**, *37* (10), 2296−2301.
(72) Lorenzetti, M.; Dogša, I.; Stošicki, T.; Stopar, D.; Kalin, M.; Kobe, S.; Novak, S. The Influence of Surface Modification on Bacterial Adhesion to Titanium-Based Substrates. *ACS Appl. Mater. Interfaces* **2015**, *7* (3), 1644−1651.
(73) Gonzalez Arellano, D. L.; Kolewe, K. W.; Champagne, V. K.; Kurtz, I. S.; Burnett, E. K.; Zakashansky, J. A.; Arisoy, F. D.; Briseno, A. L.; Schiffman, J. D. Gecko-Inspired Biocidal Organic Nanocrystals Initiated from a Pencil-Drawn Graphite Template. *Sci. Rep.* **2018**, *8* (11618), 1−8.

https://doi.org/10.1021/acssuschemeng.4c02806
ACS Sustainable Chem. Eng. XXXX, XXX, XXX−XXX